Applied Geochemistry 113 (2020) 104503

Contents lists available at ScienceDirect

Applied Geochemistry

journal homepage: http://www.elsevier.com/locate/apgeochem

Experimental study of shale-fluids interaction during oxidative dissolution with hydrogen peroxide, sodium hypochlorite and sodium persulfate

Yilian Li [a], Sen Yang [a], Danqing Liu [a,b,*], Cong Yang [a], Zhe Yang [a], Hai Li [c], Zhi Tang [a]

[a] School of Environmental Studies, China University of Geosciences, Wuhan, 430074, China
[b] State Key Laboratory of Biogeology and Environmental Geology, China University of Geosciences, Wuhan, 430074, China
[c] Wuhan Centre of China Geological Survey, Wuhan, 443003, China

ARTICLE INFO

Editorial handling by Dr T. H. Darrah

Keywords:
Shale
Organic matter
Pyrite
Oxidative dissolution
Water chemistry

ABSTRACT

The drastic decline of shale gas production after fracturing depresses the development of this unconventional gas resource. Although shale oxidant stimulation can dissolve unstable composition to enhance permeability, the shale-fluids interaction during this stimulation process is still not yet clear. In this study, the organic-rich shale collected from the Cambrian Shuijingtuo Formation of Yichang, Hubei province, China was selected to react with three oxidants, hydrogen peroxide (H_2O_2), sodium hypochlorite (NaClO) and sodium persulfate ($Na_2S_2O_8$) at formation temperature. Variation of water chemistry, mineral composition and micromorphology were analyzed to reveal the mechanism of shale oxidative dissolution and evaluate its influence on shale permeability enhancement. Results showed that pyrite and OM can be discrepantly oxidized with different oxidants. At the same oxidation duration, the acidic environment was beneficial for carbonate dissolution, while the alkaline environment was favorable to the dissolution of dolomite and tectosilicate minerals such as quartz, albite, illite and chlorite. Nevertheless, the serious thermal decomposition of H_2O_2, precipitation of gypsum and ferric hydroxide ($Fe(OH)_3$) occurred during shale-fluids interaction at formation temperature might impede the enhancement of shale permeability. The oxidative dissolution of shale also brought about the release of trace elements, which might result in groundwater pollution. For the in-situ application of shale oxidative dissolution, difficulties such as thermal decomposition, secondary minerals precipitation and possible groundwater pollution should be considered further in the future.

1. Introduction

Over the past few decades, energy shortage and climate change have become much more serious with high global economy development (Edenhofer and Seyboth, 2013; EIA, 2018; Parmesan, 2006). As one of the efficient unconventional natural gas resources, the upsurge of shale gas development occurs after its successful commercial exploitation in North America. It is estimated that China has approximately 25 trillion cubic meters shale gas reserves (CGS, 2014), and its vigorous development is of great importance to the energy structure adjustment and environmental protection.

However, only a minority of shale gas can be directly extracted from shale reservoir due to the ultra-low permeability of shale matrix. The shale fracturing technology such as hydraulic fracturing, liquefied petroleum gas (LPG) fracturing and carbon dioxide (CO_2) fracturing, can effectively increase matrix diffusivity and enhance shale gas recovery (Liu et al., 2017; Pei et al., 2015; Rahm, 2011). Nevertheless, all these technologies are hard to realize the transformation of shale matrix and promote desorption of adsorbed gases in shale, resulting in the rapid gas production decline after shale fracturing (Karra et al., 2015; Liu et al., 2019; Middleton et al., 2015; Moniz et al., 2011).

Shale originates from the reducing environment in deep strata, being rich in brittle minerals (e.g., quartz, feldspar), clay minerals (e.g., kaolinite, illite, and chlorite), carbonate (e.g., calcite, dolomite), pyrite and organic matter (OM). Extensive studies show that the mineral composition and structure changes during shale-fluids (e.g., water, slickwater, liquid/supercritical CO_2) interaction are quite related to fluid composition and shale geochemistry (Dieterich et al., 2016; Liu et al., 2016; Wang et al., 2015; Wilke et al., 2015). For example, when an acidic fluid such as hydrochloric acid, sulfuric acid or liquid/-supercritical CO_2 is introduced into shale, more obvious carbonate dissolution and secondary minerals precipitation could be observed (Liu

* Corresponding author. School of Environmental Studies, China University of Geosciences, Wuhan, 430074, China.
E-mail address: liudq@cug.edu.cn (D. Liu).

https://doi.org/10.1016/j.apgeochem.2019.104503
Received 8 May 2019; Received in revised form 2 September 2019; Accepted 16 December 2019
Available online 17 December 2019

et al., 2012; Paukert Vankeuren et al., 2017; Phan et al., 2018). The effect of shale-fluids interaction on shale porosity and permeability is quite dependent on whether the dominant mechanism is carbonate dissolution or clay mineral release, which is relevant to shale mineral composition (Ao et al., 2017; Jiang et al., 2016; Liu et al., 2012; Yu et al., 2012; Zou et al., 2018).

Owing to the existence of unstable composition, such as pyrite and OM, shale permeability enhancement through oxidative dissolution attracts more attention recently. Kuila et al. (2014) found that OM in mudrock was easily oxidized by sodium hypochlorite (NaClO), and the clay-hosted porosity increased after OM removal. Dissolution of carbonate, pyrite, chlorite and OM, as well as the generation of oxidation-induced fractures were observed by Chen et al. (2017a) when they compared the composition and pore structure of Longmaxi black shale before and after 15 wt % hydrogen peroxide (H_2O_2) treatment. Similarly, Zhou et al. (2018) also found the reaction between OM and H_2O_2 led to the increase of shale porosity, but the mineral composition remained unchanged. The different changes of mineral composition implied that the mineral assemblage significantly affected the shale-fluids interaction. Studies of coal oxidation with NaClO, potassium permanganate ($KMnO_4$), H_2O_2 and potassium persulfate ($K_2S_2O_8$) indicated their stimulation for coal seam permeability enhancement, which provided another evidence for enhancing shale permeability with oxidative dissolution (Doskočil et al., 2014; Jin et al., 2011; Jing et al., 2018a, 2018b). However, all these studies were carried out at ambient temperature, and water chemistry which reflected the shale-fluids interaction mechanism and evaluated potential groundwater pollution was neglected (Harrison et al., 2017; Marcon et al., 2017; Marcon and Kaszuba, 2015; Yang et al., 2015).

Therefore, the purpose of this study is to: 1) reveal the mechanism of shale-fluids interaction during shale oxidative dissolution, 2) evaluate the feasibility of shale oxidative dissolution with different oxidants at formation temperature. The Cambrian Shuijingtuo shale is chosen for this study because of its distinct geological characteristics and mineral composition with the Silurian Longmaxi shale in Sichuan Basin and Triassic Yanchang shale in Ordos Basin (Chen et al., 2018). Shale oxidative dissolution experiments with different oxidants are carried out to accomplish the two goals. Combining XRD, SEM and TOC analysis, the interaction mechanism between different oxidants and shale was illustrated through water chemistry, mineral composition and micromorphology variation of shale.

2. Material and methods

2.1. Shale sample preparation

High shale gas industry flow obtained from Cambrian Shuijingtuo Formation of Yichang, Hubei province, central China denotes a

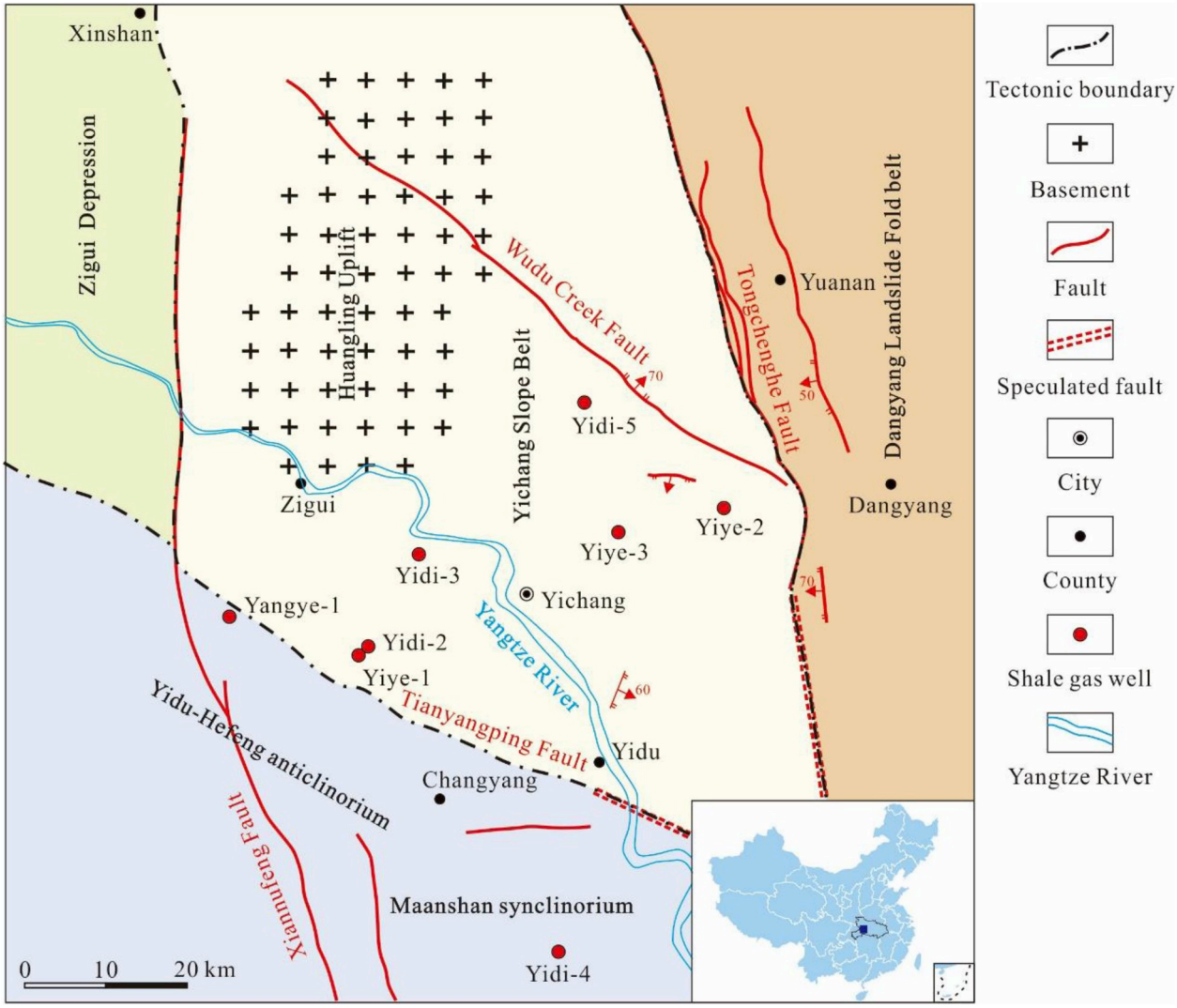

Fig. 1. Geologic map and location of shale gas wells in Yichang, Hubei province, central China.

significant breakthrough in marine shale gas exploitation in south China (Chen et al., 2017b). Yichang is located on the southeastern margin of Huangling uplift in the middle Yangtze platform, which has stable structures and good preservation conditions for shale gas (Chen et al., 2018). The lower Cambrian Shuijingtuo shale (~1854 m) used in this study was collected from the Yiye-1 well of Yichang area (Fig. 1). Different from Silurian Longmaxi Formation and Triassic Yanchang Formation, the Shuijingtuo shale are generally characterized by high calcium and low silicon, as well as medium TOC content (Table 1).

Samples were crushed and sieved to a particle size of 150–600 μm. The crushed samples were divided into seven groups: one group was fresh samples, the others were used for shale oxidative dissolution at different times. All crushed samples were dried at 60 °C for 48 h before all experiments.

2.2. Oxidative dissolution experiments

To simulate reservoir conditions, the oxidative dissolution experiments were carried out at reservoir temperature (60 °C) and atmospheric pressure. The atmospheric pressure was chosen due to security and its negligible effect on minerals solubility (Morel and Hering, 1993). Three different oxidants, H_2O_2 (15 wt %), NaClO (1.6 M, which contains 5.68 g active chlorite, 7.8 g sodium hydroxide and 32 g sodium bicarbonate per 100 mL solution) and sodium persulfate ($Na_2S_2O_8$, 1 M) were used for shale oxidative dissolution experiments. Each 2 g shale was added into 40 mL solution (Deionized water or oxidants) in a 250 mL Teflon conical flask for experiments. The flasks were divided into six groups and shaken at 60 °C on an oscillator (180 rpm) for 5, 10, 24, 48, 72 and 120 h, respectively. After the experiments, the solutions with residues were transferred into the 50 mL polypropylene centrifuge tubes for centrifugation (4000 rpm, 5 min). Then the supernatants were divided into two parts, one aliquot of supernatants were used for pH (PB-10, Sartorius, Germany) determination immediately, and the others were filtered and collected for ions analysis. The residues were washed with deionized water and followed by centrifugation five times to remove the dissolved salts. Then the cleaned residues were dried at 60 °C for 48 h and collected for the analysis of shale mass loss, TOC, mineralogy and micromorphology.

2.3. Measurement of total organic carbon content

The TOC content of untreated and treated shale samples was measured by TOC Analyzer (Elementar Vario, Germany). Prior to analysis, all shale samples were crushed and passed through 100 mesh (<150 μm) sieve. Sufficient hydrochloric acid was used to react with samples to remove carbonate before TOC analysis.

2.4. Mineralogy and micromorphology characterization

The mineral composition of all shale samples was analyzed by X-ray diffraction (XRD, D8-FOCUS, Bruker Company, Germany) with Cu Kα radiation after they were crushed and passed through 200 mesh (<75 μm) sieve. All samples were scanned from 5° to 90° with a scanning rate of 10°/min and a step size of 0.01°. Then the mineral composition of shale samples was quantitatively determined by the reference intensity ratio method (Hillier, 2000). The micromorphology change and element distribution of shale were imaged by scanning electron microscopy (SEM, SU800, Hitachi, Japan) with energy dispersive spectroscopy (EDS). Images were collected based on an accelerating voltage of 10–25 kV after samples coated by gold.

2.5. Water chemistry analysis

The filtered supernatants were divided into four parts, which were used for concentration measurements of Fe(II + III), oxidants, cations and anion, respectively. To avoid the Fe(II) oxidation and oxidants decomposition, the concentrations of Fe(II), Fe(III) and oxidants were measured immediately after sampling. Samples tested for cations were acidified with 2 wt % nitric acid. Concentrations of Fe(II) and Fe(III) after oxidative dissolution experiments were determined by the 1,10-phenanthroline method at 510 nm using a UV–visible spectrophotometer (U-3900, Hitachi, Japan) (Tamura et al., 1974). Concentrations of oxidants including H_2O_2, NaClO and $Na_2S_2O_8$ were measured at 400 nm using a UV–visible spectrophotometer (U-3900, Hitachi, Japan) (Liang et al., 2008). The concentrations of major cations and trace elements were measured by ICP-OES (5100, Agilent, Technologies, USA) and ICP-MS (ELAN DRC-II, PerkinElmer Company, USA), separately. An internal standard, Rh, was used for ICP-MS analysis to reduce the uncertainty of measurement. The concentration of anion was measured by IC (ICS-1100, DIONEX, USA).

3. Results

3.1. Evolution of water chemistry

3.1.1. pH

As a significant factor determining the degree and direction of water-rock interaction, pH of the reaction solutions after shale treated with different oxidants was shown in Fig. 2a. Due to the buffering of carbonate minerals, pH of the H_2O_2 solution increased sharply from 4.13 to 7.61, then remained stable in weakly alkaline condition over time. Compared to H_2O_2, the pH of NaClO and $Na_2S_2O_8$ solutions was quite disparate. The pH of NaClO solution showed a minor variation between 13.5 and 14.0 during the oxidation process, remaining at strong alkalinity environment due to the existence of sodium hydroxide and sodium bicarbonate in solution. Conversely, pH of the $Na_2S_2O_8$ solution declined slowly from 1.28 to 0.46 and then became rather stable in the strong acid environment. The discrepancy of pH in solutions with different oxidants resulted in diverse shale-fluids interactions.

3.1.2. Oxidant

The residual concentration ratio (R) of oxidants during shale oxidative dissolution was shown in Fig. 2b. Concentrations of all oxidants decreased sharply before reaching a relative slow reduction tendency. Among the three oxidants, the concentration of H_2O_2 showed a dramatic decrease within 5 h and was undetectable after 24 h treatment, which was ascribed to the severe thermal decomposition of H_2O_2 (Williams, 1928). The NaClO concentration showed a 59.9% decrease after 5 h treatment, higher than that of 33.9% in $Na_2S_2O_8$. This can be caused by the differences in the oxidation efficiency of the two oxidants, as well

Table 1
Comparison of shale mineral composition and TOC content.

Sample	type	TOC content (wt %)	Mineralogical compositions (wt %)							Source
			Quartz	Calcite	Dolomite	Clay	Feldspar	Pyrite	Siderite	
Shuijingtuo shale	core	4.64	36.8	25.6	5.5	22.2	5.8	4.1	0.0	This study
Longmaxi Shale	outcrop	4.00	53.5	0.0	2.2	31.9	7.6	2.6	2.2	Chen et al. (2017a)
Longmaxi Shale	outcrop	4.02	57.4	3.8	5.7	24.9	5.8	2.4	0.0	Pan et al. (2018)
Chang 7 shale	core	5.64	23.6	3.6	2.5	47.3	20.4	2.6	0.0	Pan et al. (2018)
Chang 7 shale	core	4.32	26.6	4.1	4.0	34.3	22.7	8.3	0.0	Pan et al. (2018)

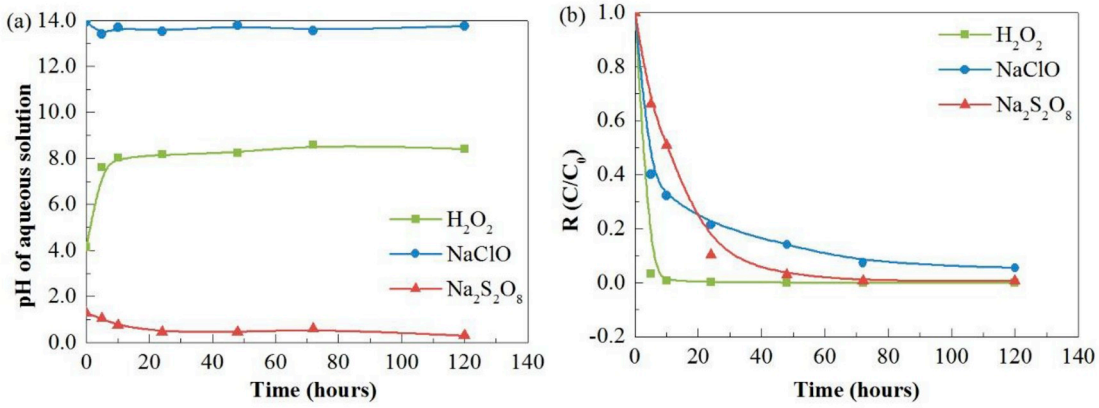

Fig. 2. (a) Solutions pH variatioin with different oxidants treatment; (b) Residual concentration ratio (R) of oxidants over time. R is calculated as C/C_0, where C and C_0 are the current and initial concentration of oxidants in solution, separately.

as the partial thermal decomposition of NaClO at the experimental temperature. $Na_2S_2O_8$ had the maximum R value among three oxidants after 5 h treatment due to its thermal stability. Then, the R value of $Na_2S_2O_8$ significantly decreased from 0.66 to 0.10 at the reaction time from 5 to 24 h, indicating its large consumption during minerals dissolution at the acid environment.

3.1.3. Major ions

Fe, which mainly originated from pyrite in shale, can be used to reflect the oxidation mechanism of various oxidants. Concentrations of different Fe species during the oxidation process were plotted in Fig. 3a. There were seldom Fe(II) and Fe(III) in H_2O_2 solutions, which might be ascribed to the thermal decomposition of H_2O_2 and precipitation of iron hydroxide ($Fe(OH)_3$). The Fe(II) concentrations in NaClO and $Na_2S_2O_8$ solutions were quite similar, while that of Fe(III) increased significantly with time during $Na_2S_2O_8$ treatment but remained quite small with NaClO treatment. Precipitation of $Fe(OH)_3$ at the strong alkaline environment can be inferred from the different concentrations of Fe(III) in $Na_2S_2O_8$ and NaClO solutions after treatment. Sulfate ion was another product of pyrite oxidation, the concentration of which was shown in Fig. 3b. The concentration of sulfate ion in NaClO was larger than H_2O_2, which illustrated much more pyrite being oxidized by NaClO than H_2O_2 at the experimental condition.

The evolution of other cations after treatment with different oxidants was shown in Fig. 4. The concentrations of K, Mg and Ca in $Na_2S_2O_8$ solutions showed a significant increase at first, then the ascending rate became slowly over time, while the concentration of Al in $Na_2S_2O_8$ solutions increased linearly with time. Distinct concentration and release rate among K, Mg, Ca and Al demonstrated that the dissolution rate of shale minerals such as carbonate and clay minerals were quite different at the strong acid environment. Compared to $Na_2S_2O_8$, the concentrations of K, Na, Mg and Al in H_2O_2 solutions were rather small, while that of Ca was comparable. Different from $Na_2S_2O_8$ and H_2O_2, seldom Ca and Mg occurred in NaClO, but the abundant K and Si, as well as the less amount of Al, appeared in NaClO solutions, indicating the dissolution of quartz and clay minerals rather than carbonate.

3.1.4. Trace elements

The 120 h treatment of shale with different oxidants resulted in diverse trace elements mobilization (Fig. 5). After the experiments, limited concentrations of trace elements were detected in H_2O_2 solution, and it was quite similar to deionized water treatment. High mobility of As, Ba, Cr and V was observed in NaClO and $Na_2S_2O_8$ solutions, while the concentrations of Cu, Ni, Rb and U in $Na_2S_2O_8$ solution were higher than NaClO solution after the experiment.

3.2. Shale composition variation

3.2.1. Mass loss

Mass loss of shale before and after experiments, which was shown in Fig. 6, was the quantification of water-rock interaction. The mass loss of $Na_2S_2O_8$-treated shale was increased most significantly with time and reached up to 15.27% after 120 h treatment, indicating the severe dissolution of OM and mineral. Although the mass loss curve of H_2O_2-treated shale was similar to the study of Chen et al. (2017a) at room temperature, only about half of the magnitude occurred in this study due to the thermal decomposition of H_2O_2. Interestingly, the mass loss of NaClO-treated shale increased first and then decreased over time, which

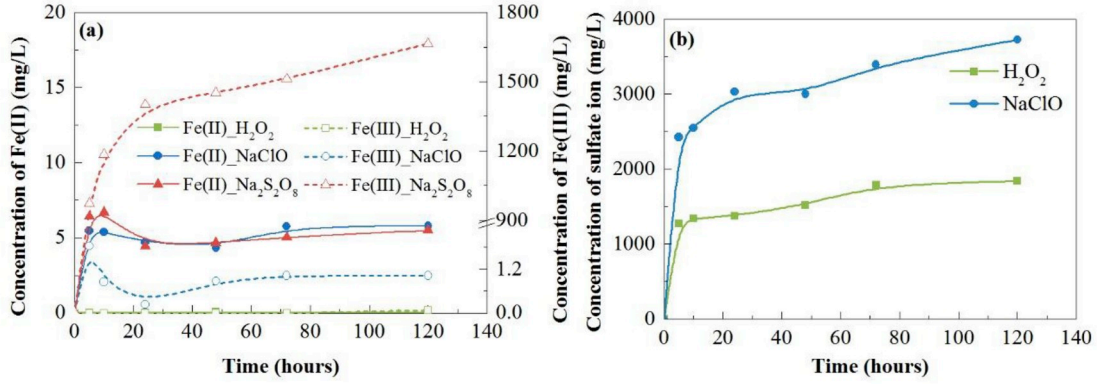

Fig. 3. The concentration of (a) Fe in different species and (b) sulfate ion during the oxidation process (Concentration of sulfate in $Na_2S_2O_8$ solutions was not shown due to its inherent high concentration.).

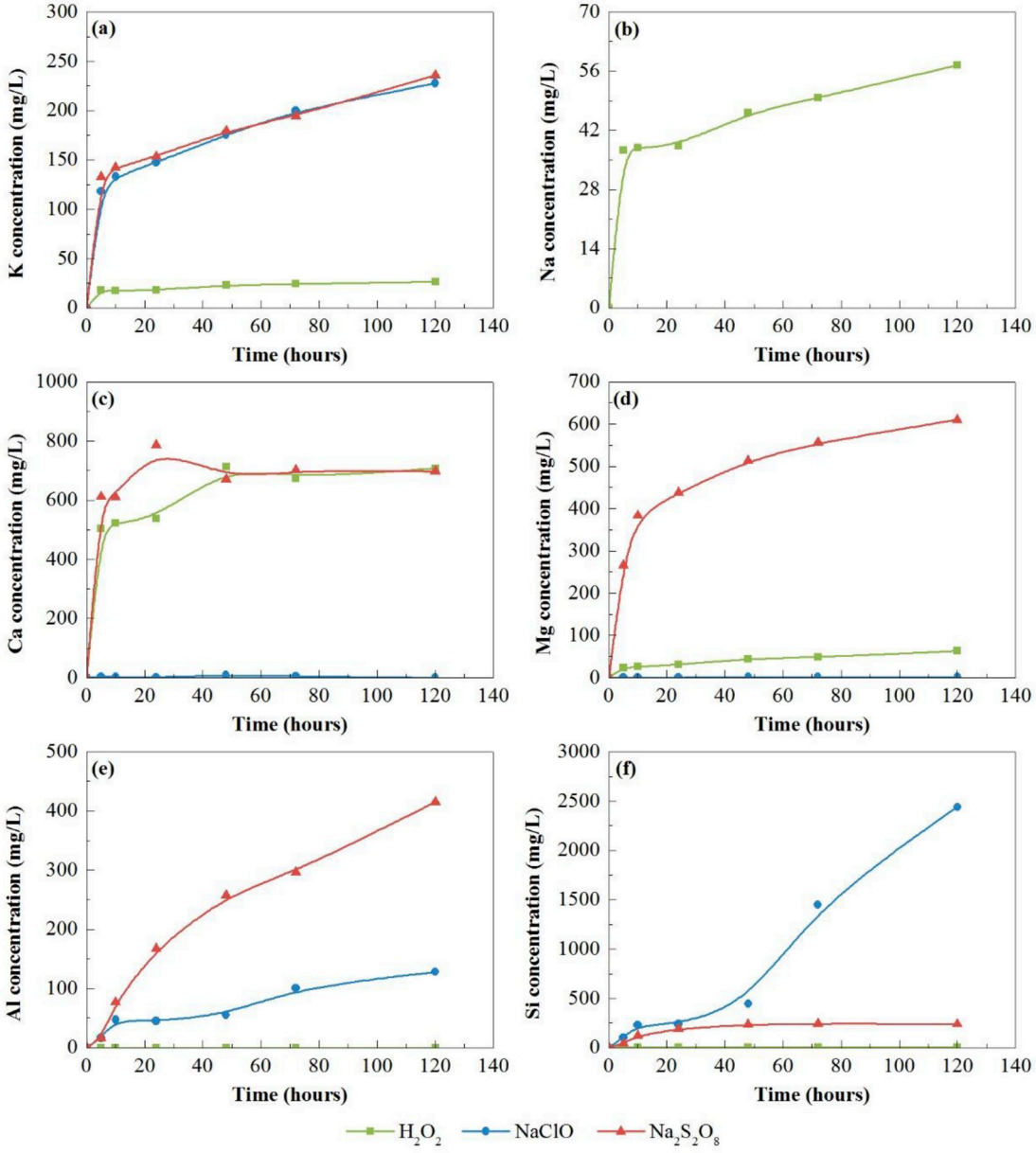

Fig. 4. The concentration of major cations during oxidation process (Concentrations of Na in NaClO and $Na_2S_2O_8$ solutions were not shown due to their inherent high concentration.).

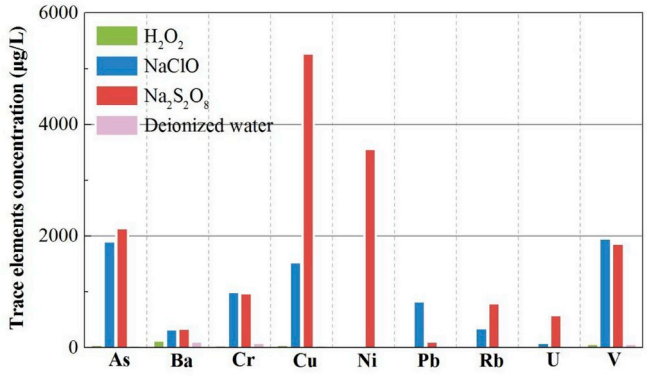

Fig. 5. Trace elements concentration after 120 h treatment with different oxidants.

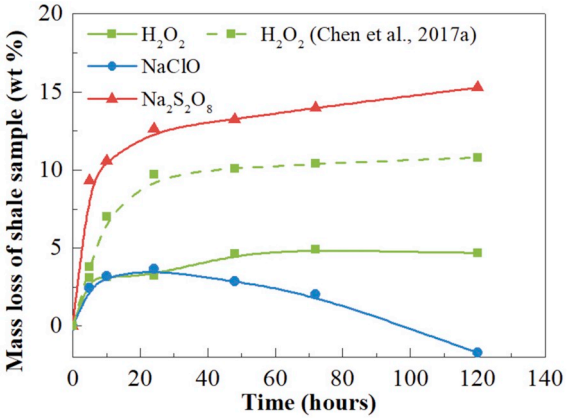

Fig. 6. Mass loss of shale with time for different oxidants treatment.

might be caused by the precipitation of secondary mineral in the strong alkaline environment.

3.2.2. Change of mineral composition

To reveal the mechanism of shale-oxidants interaction, the alternation of shale mineral phases after 120 h treatment was measured with XRD (Fig. S1). Quantitative analysis showed that the untreated Shuijingtuo shale has a mineralogical composition of 32.3 wt % illite, 25.0 wt % quartz, 14.7 wt % calcite, 11.4 wt % albite, 8.0 wt % chlorite, 5.4 wt % pyrite and 3.2 wt % dolomite (Table 2). The declined content of calcite (10.5 wt %), dolomite (2.0 wt %) and pyrite (3.4 wt %) was observed after H_2O_2 treatment, while the diffraction peak of pyrite even disappeared in NaClO and $Na_2S_2O_8$-treated shale. Moreover, a large amount dissolution of calcite, dolomite and chlorite, as well as precipitation of gypsum were observed after $Na_2S_2O_8$ treated shale. The distinct change of relative content of minerals indicated the differential shale-fluids interaction during shale oxidative dissolution in different oxidant solutions.

3.2.3. Change of organic matter content

The TOC content of shale was used for its OM quantification, whose variation was shown in Fig. 7a. The TOC of untreated shale was 4.64 wt % and declined distinctly with time after different oxidants treatment. Furthermore, all TOC content remained stable after 24 h decreasing, indicating the fast OM oxidation rate at the experimental condition. The removal efficiency of TOC with NaClO oxidation was 74.77%, larger than that of H_2O_2 (11.08%) and $Na_2S_2O_8$ (28.63%) (Table 3). To clarify the discrepancy of TOC decline with different oxidants, the TOC decrease rate was calculated and shown in Fig. 7b. The descending TOC decrease rates were shown in NaClO-treated shale, and the same phenomenon could be observed in H_2O_2-treated shale at the first 24 h. However, a peak TOC decrease rate occurred in $Na_2S_2O_8$-treated shale, indicating the slow OM oxidation rate at the first 5 h treatment. The non-monotonic TOC decrease rate of $Na_2S_2O_8$-treated shale suggested that the dissolution of minerals at the first 5 h were more conducive to shale OM exposure and oxidation, indicating the benefit of rapid mineral reaction on OM oxidation under acidic condition.

3.3. Micromorphology variation of shale

SEM images showed that the micromorphology of untreated shale was dominated by angular grains before oxidative dissolution (Fig. 8a). The presence of carbonate (Fig. 8b), pyrite (Fig. 8c), clay mineral (Fig. 8d) and organic matter (Fig. 8e) were qualitatively confirmed by the element composition from EDS analysis (Fig. 8f).

After interaction with H_2O_2, the edge and surface of carbonate became smoother and were attached by much small debris (Fig. 9a and e), indicating the partial dissolution of carbonate at the weak acid environment. Based on the SEM-EDS results of H_2O_2-treated shale, the new spherical flocs were mainly comprised of Fe and O, confirming the oxidative dissolution of pyrite and the precipitation of $Fe(OH)_3$ (Fig. 9b and e). After NaClO treatment, the crystal shape of clay mineral changed from angular to spherical, while the mineral surface attached with new minerals (Fig. 9c). With the analysis of SEM-EDS, it might be the coexistence of clay mineral dissolution and $Fe(OH)_3$ precipitation (Fig. 9e). Due to a large amount of Ca dissolution from carbonate and S input in $Na_2S_2O_8$ solution, well-crystallized gypsum was observed in shale after $Na_2S_2O_8$ treatment (Fig. 9d and e).

To further clarify the effect of different oxidants on pyrite oxidation, the images of shale samples and the distribution of the corresponding element of Fe and S in untreated and treated shales were shown in Figs. S2 and S3. The aggregation and coexistence of element Fe and S in some locations not only indicated the abundant pyrite in untreated shale but also confirmed its incomplete dissolution in the H_2O_2 solution (Figs. S3a and S3b). After the treatment of NaClO, the distribution of element Fe and S was rather homogeneous, indicating the complete dissolution of pyrite. Comparing with NaClO-treated shale, similar but rather less density of Fe occurred in $Na_2S_2O_8$-treated shale, demonstrating the Fe release from pyrite oxidation in $Na_2S_2O_8$ (Fig. S3d) as well as the precipitation of $Fe(OH)_3$ in NaClO (Fig. S3c). Moreover, it was also evident that the enriched S in shale after $Na_2S_2O_8$ treatment was ascribed to the precipitation of gypsum (Fig. S3d).

Table 2
Mineral content of untreated and different oxidants treated samples from X-ray diffraction patterns.

Mineral	Untreated (wt %)	H_2O_2 treated (wt %)	NaClO treated (wt %)	$Na_2S_2O_8$ treated (wt %)
Quartz	25.0	29.8	30.7	23.7
Calcite	14.7	10.5	16.0	0.0
Dolomite	3.2	2.0	1.3	0.0
Illite	32.3	34.1	31.0	36.8
Chlorite	8.0	7.9	8.4	0.0
Albite	11.4	12.3	12.6	7.6
Pyrite	5.4	3.4	0.0	0.0
Gypsum	0.0	0.0	0.0	31.9

4. Discussion

4.1. Oxidation, dissolution and precipitation of minerals

4.1.1. Oxidation of pyrite

The ubiquitous pyrite in shale forms from the anoxic environment, and is easily oxidized when exposed to atmosphere or water contained oxygen, not to mention other oxidants (Moses and Herman, 1991; Moses et al., 1987). Reactions between pyrite and oxidants can be generally represented as follows:

$$2FeS_2 + 15H_2O_2 \rightarrow 2Fe^{3+} + 4SO_4^{2-} + 2H^+ + 14H_2O \quad (1)$$

$$2FeS_2 + 15ClO^- + 8OH^- \rightarrow 2Fe(OH)_3\downarrow + 15Cl^- + 4SO_4^{2-} + H_2O \quad (2)$$

$$2FeS_2 + 15S_2O_8^{2-} + 16H_2O \rightarrow 2Fe^{3+} + 34SO_4^{2-} + 32H^+ \quad (3)$$

$$FeS_2 + 14Fe^{3+} + 8H_2O \rightarrow 15Fe^{2+} + 2SO_4^{2-} + 16H^+ \quad (4)$$

The reduction of pyrite content after shale-oxidants interaction demonstrates the feasibility of pyrite oxidation (Figs. S1, S2, S3 and Table 2), however, diverse shale-oxidants interaction result in different oxidation efficiency. Instead of little pyrite being left in shale after NaClO or $Na_2S_2O_8$ treatment, there was still 63.0% of pyrite remaining in shale under H_2O_2 oxidation. The discrepancy is consistent with the residual concentration of oxidants over time (Fig. 2b), indicating that the thermal decomposition of H_2O_2 is responsible for the low oxidation efficiency of pyrite. The shale-H_2O_2 interaction results in less major and trace elements dissolution (Figs. 3–5) when compared with the other two oxidants, which is also ascribed to the H_2O_2 decomposition. Despite the oxidation efficiency, there are discrepancies in Fe species after oxidation, which quite depends on the pH of the aqueous solution. According to the Eh-pH diagram of Fe–O–H system (Brookins, 1988), the $Fe(OH)_3$ precipitation easily occurs in the neutral and alkaline environment, while the Fe(III) can only exist in an acid environment (Jew et al., 2017). Furthermore, rate of pyrite oxidation significantly increases with the elevated pH, and the soluble Fe(II)/Fe(III) carbonate complexes formed in the presence of carbonate ions facilitate the reaction rate in the pH from 8.5 to 10 (Caldeira et al., 2010; Moses and Herman, 1991). However, the strong alkaline solution of NaClO is not favorable for the formation of these soluble complexes. Thus, there are negligible Fe(II) and Fe(III) in solution after H_2O_2 and NaClO treatment (Fig. 3a), and the precipitation of $Fe(OH)_3$ occurs in the residues (Fig. 9b and c).

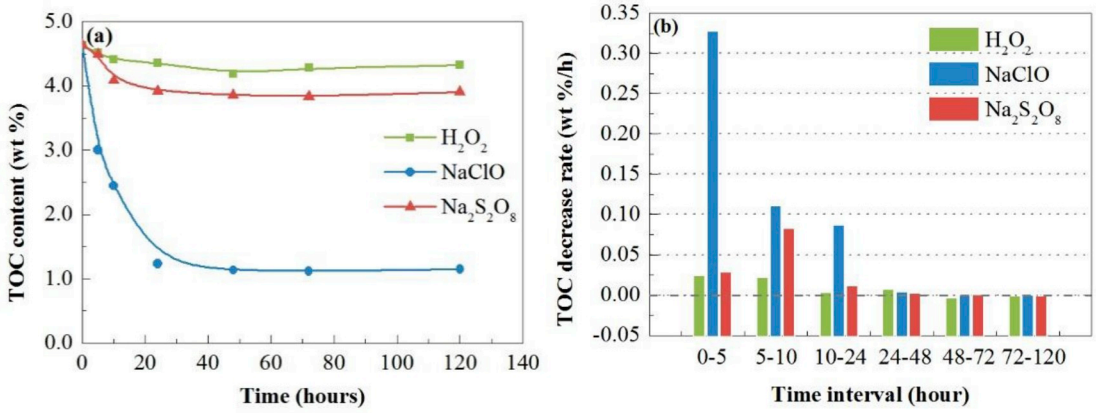

Fig. 7. (a) TOC content of shale with time for different oxidants treatment. (b) TOC decrease rate of shale with time. The Gray dash line represents no TOC variation. The rate is calculated as (Ci-Cj)/(Ti-Tj), where Ci and Cj are the TOC content of shale at the beginning and end of a certain time period, and Ti and Tj are the corresponding time.

Table 3
TOC removal efficiency of shale after 120 h oxidant treatment.

Oxidant	H_2O_2	NaClO	$Na_2S_2O_8$
TOC removal efficiency (%)	11.08	74.77	28.63

4.1.2. Minerals dissolution and precipitation in acidic environment

According to the XRD and SEM analysis, the Cambrian Shuijingtuo shale used in this study is abundant in illite, quartz, calcite and albite, while contains a small amount of chlorite, pyrite and dolomite. As proved by numerous studies, the mineral dissolution at the acidic environment can generally be described as follows (Cui et al., 2017; Du et al., 2018):

$$CaCO_3 + H^+ = Ca^{2+} + HCO_3^- \quad (5)$$

$$CaMg(CO_3)_2 + 2H^+ = Ca^{2+} + Mg^{2+} + 2HCO_3^- \quad (6)$$

$$K_{0.6}Mg_{0.25}Al_{2.3}Si_{3.5}O_{10}(OH)_2 + 8H^+ = 0.6K^+ + 0.25Mg^{2+} + 2.3Al^{3+} + 3.5SiO_2(aq) + 5H_2O \quad (7)$$

$$Mg_{2.5}Fe_{2.5}Al_2Si_3O_{10}(OH)_8 + 16H^+ = 2.5Fe^{2+} + 2.5Mg^{2+} + 2Al^{3+} + 3SiO_2(aq) + 12H_2O \quad (8)$$

$$NaAlSi_3O_8 + 4H^+ = Na^+ + Al^{3+} + 3SiO_2(aq) + 2H_2O \quad (9)$$

As the dissolution rate of carbonate (eqs. (5) and (6)) is faster than other minerals such as feldspar and clay mineral at the acidic environment, the Ca and Mg are easy to be released into $Na_2S_2O_8$ solution (Fig. 4c and d), resulting in the full dissolution of carbonate (Fig. S1 and Table 2). Compared to $Na_2S_2O_8$, the weaker acidity of H_2O_2 means that the smaller amount of carbonate dissolution can recover the pH to near-neutral (Fig. 2a). Although the reaction rate of illite, chlorite and albite are slower than carbonate, high temperature, as well as the strong acid environment, may provide favorable conditions for their dissolution. When comparing the water chemistry of solution after shale interacted with H_2O_2, a larger amount dissolution of K, Al and Si are observed in $Na_2S_2O_8$ solution, indicating the dissolution of illite, chlorite and albite. The variation of shale mineral composition after oxidative dissolution also demonstrates the significant dissolution of chlorite and albite after $Na_2S_2O_8$ treatment than H_2O_2 treatment (Fig. S1 and Table 2), which is

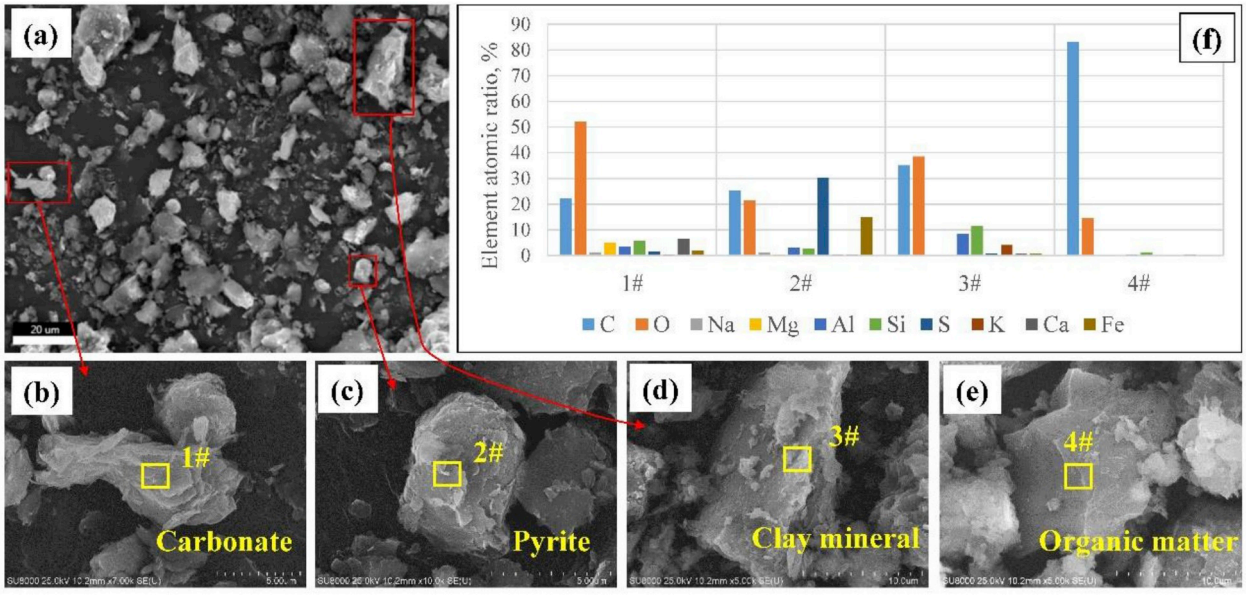

Fig. 8. The micromorphology of untreated shale and its typical minerals.

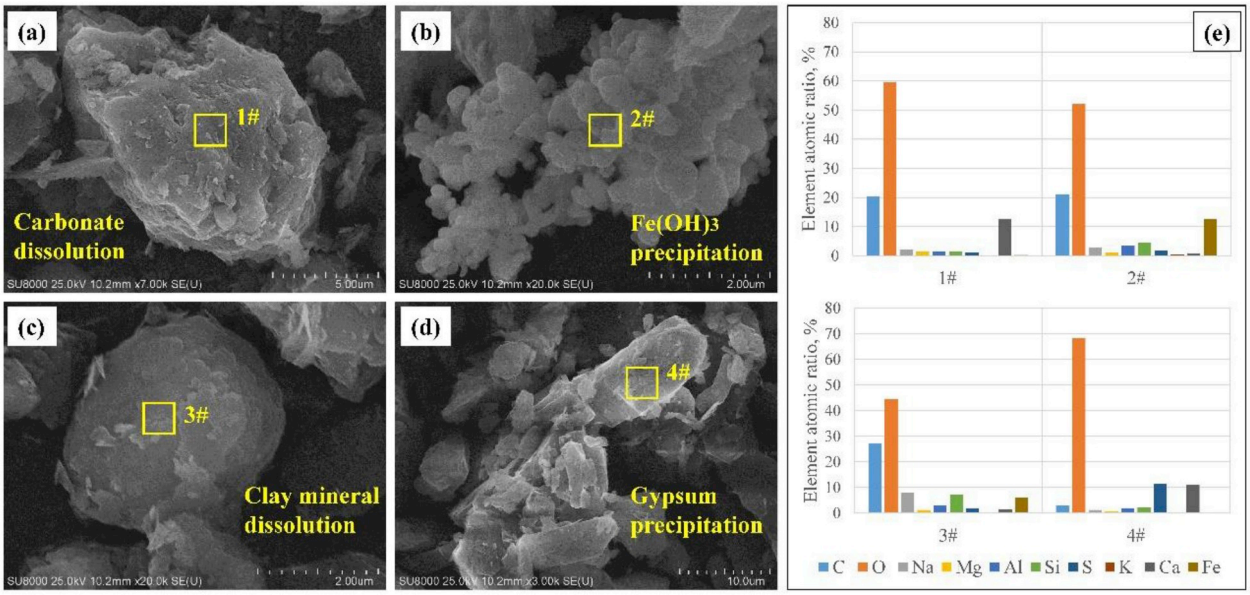

Fig. 9. The micromorphology of typical minerals after dissolution and precipitation.

ascribed to the stronger acidity of solution due to abundant sulfuric acid generation (eq. (3)). Corrosion of chlorite and K-feldspar by sulfuric acid has also previously been observed in SO_2–CO_2-water-sandstone system (Pearce et al., 2015). Besides, XRD and SEM analysis indicate the formation of gypsum in $Na_2S_2O_8$ (Figs. S1, 9d, S2d and S3d, Table 2), which is facilitated by the dissolution of carbonate. The generation of gypsum is shown as the following reaction:

$$Ca^{2+} + SO_4^{2-} + 2H_2O = CaSO_4{\cdot}2H_2O \quad (10)$$

4.1.3. Minerals dissolution and precipitation in alkaline environment

Different from H_2O_2 and $Na_2S_2O_8$, the NaClO used in this study contains sodium hydroxide and sodium bicarbonate, resulting in a high pH during shale-NaClO interaction (Fig. 2a). As a common engineering problem, the alkali-silica reaction can lead to the dissolution of quartz, feldspar and clay minerals, whose rate increases with elevated pH at the alkaline environment (Thomas, 2011). The dissolution of quartz, albite, illite and chlorite can generally be described as follows:

$$SiO_2 + 2OH^- = H_2SiO_4^{2-} \quad (11)$$

$$NaAlSi_3O_8 + 6OH^- + 2H_2O = Na^+ + Al(OH)_4^- + 3H_2SiO_4^{2-} \quad (12)$$

$$K_{0.6}Mg_{0.25}Al_{2.3}Si_{3.5}O_{10}(OH)_2 + 3H_2O + 8.7OH^- = 0.6K^+ + 0.25Mg(OH)_2\downarrow + 2.3Al(OH)_4^- + 3.5H_2SiO_4^{2-} \quad (13)$$

$$Mg_{2.5}Fe_{2.5}Al_2Si_3O_{10}(OH)_8 + 4H_2O + 8OH^- = 2.5Fe(OH)_2\downarrow + 2.5Mg(OH)_2\downarrow + 2Al(OH)_4^- + 3H_2SiO_4^{2-} \quad (14)$$

As shown in Fig. 4, K, Al and especially Si are largely released into solutions after NaClO treatment. Since they are sourced from tectosilicate minerals such as quartz, albite, illite and chlorite, it can be inferred that the dissolution of tectosilicate minerals dominates the shale oxidative dissolution process under alkaline environment. However, the relative content of minerals such as quartz, calcite, chlorite and albite increases (Table 2) after NaClO treatment, which was partially attributed to the disappearance of pyrite. In contrast, the content of dolomite decreases after the reaction, which might be ascribed to its dissolution (Kang et al., 2016; Pokrovsky, 2001). Although our study demonstrates the dissolution of tectosilicate minerals dominated the shale oxidative dissolution process in an alkaline environment, the contribution of different tectosilicate minerals during shale oxidative dissolution is still unclear. Experiments of interaction between pure minerals and oxidants will carry out in the later future to focus on this problem. Moreover, precipitation of solid phases during shale-alkali interaction has previously been reported by numerous studies, which includes the metal hydroxide, polymer of Si group and silicate (Saouma et al., 2015; Soler, 2003). High-valence cations including Ca^{2+}, Mg^{2+} and Fe^{3+} are generated from the reaction between alkali solution and minerals such as dolomite and chlorite, which tend to precipitate as metal hydroxide in the alkaline environment. In addition, the cation exchange between Na^+ and these high-valence cations in shale minerals can also generate the precipitates (Kang et al., 2016). However, as the net change of shale mass shows an increase before and after 120 h NaClO treatment, it can be concluded that some other products are generated from adsorption and complexation between silicate and cations in solutions (Saouma et al., 2015).

4.1.4. Possible mechanism of minerals and ions migration

Based on the above analysis, the oxidants properties including pH and thermal stability result in the distinct shale-fluids interaction during shale oxidative dissolution. In an acidic environment, the shale-fluids interaction is dominant by carbonate dissolution and pyrite oxidation, as well as gypsum precipitation. Instead, the interaction between shale and NaClO solution is predominantly dissolution of tectosilicate minerals. The precipitation of metal hydroxide, adsorption and complexation of cations by silicate are ascribed to the shale mass increased before and after NaClO treatment. The possible mechanism of minerals and ions migration during shale oxidative dissolution is shown as Fig. 10.

4.2. Oxidation of organic matter

The decreased TOC content of shale (Fig. 7) demonstrates the oxidation of organic matter by added oxidants, and the removal efficiency of which is 11.08%, 74.77% and 28.63% for H_2O_2, NaClO and $Na_2S_2O_8$, respectively (Table 3). Previous studies show that OM in shale can not only be adsorbed on the internal or external surface of clay mineral but also be regarded as the structural stable particulate OM or lens-shaped discrete organic layers within clay mineral (Salmon et al., 2000; Zhu et al., 2016). When shale interacted with oxidants, the occurrence state alternation of OM or chemical bonds destruction between OM and minerals results in the OM escape from shale. However, the metal cations on the external surface of clay minerals can interact

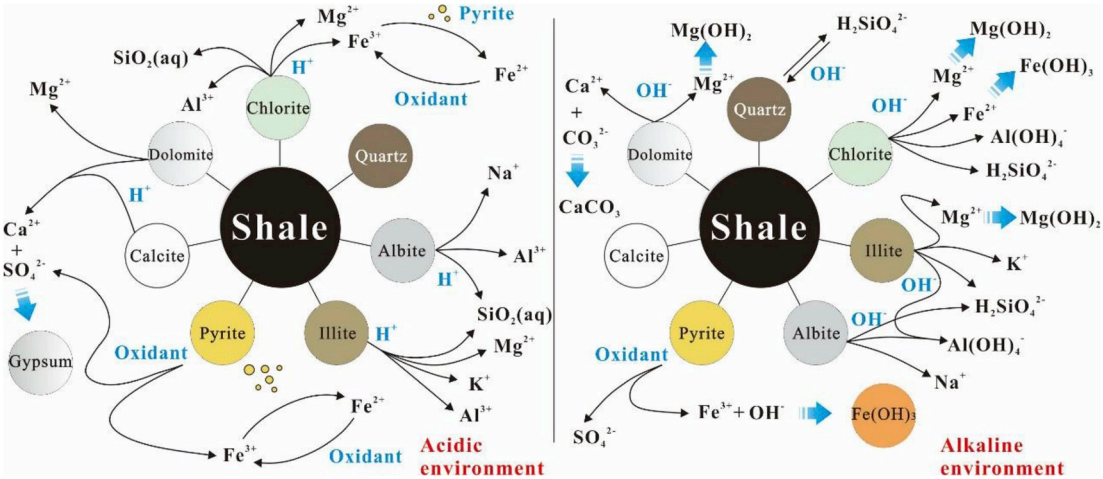

Fig. 10. Possible mechanism of minerals and ions migration in shale oxidative dissolution.

with OM through ligand exchange, cation bridging and surface complexing, to mitigate OM from oxidation. This metal cations protection capability on clay mineral as well as the existence of stable OM causes the incomplete removal of OM, which is responsible for the 25.23% TOC residual in NaClO treated shale (Fig. 7).

Compared with NaClO, the TOC removal efficiency of shale after 120 h H_2O_2 and $Na_2S_2O_8$ treatments remain rather low. The high TOC residual after H_2O_2 treatment is consistent with water chemistry variation in H_2O_2 treated solutions, which ascribes to the thermal decomposition of H_2O_2. Different from H_2O_2, $Na_2S_2O_8$ is an effective oxidant for organic compounds degradation after activation of heat or alkali (Manz and Carter, 2018; Zhang et al., 2017). However, the low TOC removal efficiency occurs in this study despite the high temperature (60 °*C*) that can be explained as follows. On one hand, previous studies show the OM of Cambrian Shuijingtuo shale in Yichang is banded or encapsulated in primary minerals, such as clay minerals, calcite, pyrite and especially quartz (Chen et al., 2018). The microcrystalline quartz aggregates provide enough pore space for the filling of migrated OM such as bitumen (Zhao et al., 2017). As an acid resistance mineral, the quartz effectively protects intercalated OM from oxidative dissolution. Also, the low pH of the aqueous solution may prevent the OM desorption from the mineral surface (Jing et al., 2018a; Mikutta et al., 2005). Thus, a detailed investigation of $Na_2S_2O_8$ activated by alkali to oxidize OM in shale should be carried out in the future.

4.3. *Applicability of shale oxidative dissolution on gas shale stimulation*

Previous studies illustrate that H_2O_2 can effectively oxidize OM and pyrite as well as generate acid to increase induced fractures in shale at room temperature (Chen et al., 2017a; Zhou et al., 2018). However, the shale formation used for gas production is deeply buried underground with high temperature. The increasing ambient temperature with depth may result in the H_2O_2 decomposition before reaching the terminus. The weak shale-H_2O_2 interaction in our study makes it doubtful to enhance shale permeability.

The high TOC removal efficiency in NaClO is consistent with the OM oxidation of mudrock and permeability enhancement of coal (Table 3) (Jing et al., 2018a, 2018b; Kuila et al., 2014). Nevertheless, mass loss (Fig. 6) of shale after NaClO treatment tends to decrease due to the precipitation of secondary minerals, which might result in the permeability reduction. Since the NaClO solution has a high pH value, many major elements (Fe, Ca, Mg, Al) and trace elements (Cr, Cu, Ni, Pb and U) may precipitate with hydroxyl in a strongly alkaline environment. Similarly, although $Na_2S_2O_8$ induces an acid solution, the large amount of S in solution and Ca oxidized by carbonate are beneficial for gypsum generation (Figs. S1, 9d, S2d and S3d, Table 2). The effect of precipitation after shale oxidative dissolution on shale permeability requires in-depth research.

Due to the interaction between shale and oxidants, groundwater pollution is another problem that should be taken into further consideration. As shown in Fig. 5, the mobility of trace elements in shale has been increased after interacted with oxidants. It is reported that the trace element mobilization is not only affected by its content and occurrence, but also subjected to experimental conditions including temperature, pressure, pH and Eh (Dustin et al., 2018; Harrison et al., 2017; Wang et al., 2016). Owing to the pH and thermal stability difference of the candidate oxidants, the diverse mechanism (Fig. 10) between shale and different oxidants results in a distinct release of trace elements. Previous studies demonstrate the trace element partitioning in various minerals. For example, As and Ni mainly exist in sulfur-bearing minerals, while Cr and V are both enrich in silicate minerals and oxides (Bai et al., 2018; Luo et al., 2019). These different occurrences of trace elements will be released into solution with minerals dissolution during shale oxidation. Furthermore, the previous study also found that the a large number of heavy metals can release from shale OM such as kerogen after oxidation, and the type of OM, composition and pH of fluids both affect the release amount of trace elements (Dustin et al., 2018). Excessive release of trace elements then will lead to groundwater contamination (Akob et al., 2015; Marcon et al., 2017). Although oxidative dissolution is regarded as one of the sustainable development technology for enhancing shale gas recovery, the optimized strategy, aiming at increasing shale permeability with less environmental contamination, needs to be further studied.

5. Conclusions

The shale oxidative dissolution experiments with three different oxidants, H_2O_2, NaClO and $Na_2S_2O_8$, were carried out at formation temperature to illustrate the shale-fluids interaction mechanism and estimate its feasibility of enhancing shale permeability. The solution water chemistry, solid mineralogy and micromorphology characterization, TOC content and mass loss were analyzed and the results demonstrated that:

1. The pyrite and OM could be oxidized by all candidate oxidants, however, the oxidation efficiency was not only related to the property of the oxidants (e.g. thermal stability, pH), but also depended on the occurrence of unstable composition in shale.
2. The extra-added oxidants could result in complicated shale-fluids interaction, which leaded to the minerals dissolution and secondary minerals precipitation. The reaction was dominant by carbonate dissolution as well as gypsum precipitation in the acidic

environment, while a large amount of hydroxyl in alkaline environment promotes the dissolution of dolomite and tectosilicate minerals such as quartz, albite, illite and chlorite, as well as precipitation of secondary minerals. The shale permeability variation, which might be seriously affected by the dissolution and precipitation of the minerals, still needs precise assessment in the laboratory as well as in-situ.

3. The oxidative dissolution of shale, especially OM and pyrite, would release trace elements and result in groundwater contamination. This environmental problem should be taken into consideration before the shale oxidative dissolution technology can apply for gas shale stimulation.

Acknowledgements

This work was supported by the National Natural Science Foundation of China (NSFC, No. 41572233, No. 41902253), the China Postdoctoral Science Foundation funded project (No. 2018M632943). The authors also thank Wuhan Center of China Geological Survey for providing the shale cores for this work.

Appendix A. Supplementary data

Supplementary data to this article can be found online at https://doi.org/10.1016/j.apgeochem.2019.104503.

References

Akob, D.M., Cozzarelli, I.M., Dunlap, D.S., Rowan, E.L., Lorah, M.M., 2015. Organic and inorganic composition and microbiology of produced waters from Pennsylvania shale gas wells. Appl. Geochem. 60, 116–125.
Ao, X., Lu, Y., Tang, J., Chen, Y., Li, H., 2017. Investigation on the physics structure and chemical properties of the shale treated by supercritical CO_2. J. CO2 Util. 20, 274–281.
Bai, J., Song, K., Chen, J., 2018. The migration of heavy metal elements during pyrolysis of oil shale in Mongolia. Fuel 225, 381–387.
Brookins, D.G., 1988. Eh-pH Diagrams for Geochemistry. Springer, Berlin Heidelberg, Berlin.
Caldeira, C.L., Ciminelli, V.S.T., Osseo-Asare, K., 2010. The role of carbonate ions in pyrite oxidation in aqueous systems. Geochem. Cosmochim. Acta 74, 1777–1789.
CGS, 2014. Investigation Report on Shale Gas Resources in China. China Geological Survey, Beijing, China.
Chen, Q., Kang, Y., You, L., Yang, P., Zhang, X., Cheng, Q., 2017a. Change in composition and pore structure of Longmaxi black shale during oxidative dissolution. Int. J. Coal Geol. 172, 95–111.
Chen, X., Wang, C., Liu, An, Luo, S., Li, H., Wei, K., 2017b. The discovery of the shale gas in the cambrian Shuijingtuo Formation of Yichang area, Hubei province. Chin. Geol. 44, 188–189.
Chen, X., Wei, K., Zhang, B., Li, P., Li, H., Liu, A., Luo, S., 2018. Main geological factors controlling shale gas reservior in the Cambrian Shuijingtuo Formation in Yichang of Hubei Province as well as its and enrichment patterns. Chin. Geol. 45, 207–226.
Cui, G., Zhang, L., Tan, C., Ren, S., Zhuang, Y., Enechukwu, C., 2017. Injection of supercritical CO_2 for geothermal exploitation from sandstone and carbonate reservoirs: CO_2–water–rock interactions and their effects. J. CO2 Util. 20, 113–128.
Dieterich, M., Kutchko, B., Goodman, A., 2016. Characterization of Marcellus Shale and Huntersville Chert before and after exposure to hydraulic fracturing fluid via feature relocation using field-emission scanning electron microscopy. Fuel 182, 227–235.
Doskočil, L., Grasset, L., Válková, D., Pekař, M., 2014. Hydrogen peroxide oxidation of humic acids and lignite. Fuel 134, 406–413.
Du, Y., Sang, S., Wang, W., Liu, S., Wang, T., Fang, H., 2018. Experimental study of the reactions of supercritical CO_2 and minerals in high-rank coal under formation conditions. Energy Fuels 32, 1115–1125.
Dustin, M.K., Bargar, J.R., Jew, A.D., Harrison, A.L., Joe-Wong, C., Thomas, D.L., Brown, G.E., Maher, K., 2018. Shale kerogen: hydraulic fracturing fluid interactions and contaminant release. Energy Fuels 32, 8966–8977.
Edenhofer, O., Seyboth, K., 2013. Intergovernmental panel on climate change (IPCC). Encycl. Energy Nat. Resour. Environ. Econ. 26, 48–56.
EIA, 2018. International Energy Outlook 2018. International Energy Agency, Washington, DC, USA.
Harrison, A.L., Jew, A.D., Dustin, M.K., Thomas, D.L., Joe-Wong, C.M., Bargar, J.R., Johnson, N., Brown, G.E., Maher, K., 2017. Element release and reaction-induced porosity alteration during shale-hydraulic fracturing fluid interactions. Appl. Geochem. 82, 47–62.
Hillier, S., 2000. Accurate quantitative analysis of clay and other minerals in sandstones by XRD: comparison of a Rietveld and a reference intensity ratio (RIR) method and the importance of sample preparation. Clay Miner. 35, 291–302.
Jew, A.D., Dustin, M.K., Harrison, A.L., Joe-Wong, C.M., Thomas, D.L., Maher, K., Brown, G.E., Bargar, J.R., 2017. Impact of organics and carbonates on the oxidation and precipitation of iron during hydraulic fracturing of shale. Energy Fuels 31, 3643–3658.
Jiang, Y., Luo, Y., Lu, Y., Qin, C., Liu, H., 2016. Effects of supercritical CO_2 treatment time, pressure, and temperature on microstructure of shale. Energy 97, 173–181.
Jin, L.e., Cao, Q., Li, J., Dong, J., 2011. Sulfur removal in coal tar pitch by oxidation with hydrogen peroxide catalyzed by trichloroacetic acid and ultrasonic waves. Fuel 90, 3456–3460.
Jing, Z., Balucan, R.D., Underschultz, J.R., Steel, K.M., 2018a. Oxidant stimulation for enhancing coal seam permeability: swelling and solubilisation behaviour of unconfined coal particles in oxidants. Fuel 221, 320–328.
Jing, Z., Mahoney, S.A., Rodrigues, S., Balucan, R.D., Underschultz, J., Esterle, J.S., Rufford, T.E., Steel, K.M., 2018b. A preliminary study of oxidant stimulation for enhancing coal seam permeability: effects of sodium hypochlorite oxidation on subbituminous and bituminous Australian coals. Int. J. Coal Geol. 200, 36–44.
Kang, Y., She, J., Zhang, H., You, L., Yu, Y., Song, M., 2016. Alkali erosion of shale by high-pH fluid: reaction kinetic behaviors and engineering responses. J. Nat. Gas Sci. Eng. 29, 201–210.
Karra, S., Makedonska, N., Viswanathan, H.S., Painter, S.L., Hyman, J.D., 2015. Effect of advective flow in fractures and matrix diffusion on natural gas production. Water Resour. Res. 51, 8646–8657.
Kuila, U., McCarty, D.K., Derkowski, A., Fischer, T.B., Topór, T., Prasad, M., 2014. Nano-scale texture and porosity of organic matter and clay minerals in organic-rich mudrocks. Fuel 135, 359–373.
Liang, C., Huang, C.F., Mohanty, N., Kurakalva, R.M., 2008. A rapid spectrophotometric determination of persulfate anion in ISCO. Chemosphere 73, 1540–1543.
Liu, D., Agarwal, R., Li, Y., 2017. Numerical simulation and optimization of CO_2 enhanced shale gas recovery using a genetic algorithm. J. Clean. Prod. 164, 1093–1104.
Liu, D., Li, Y., Agarwal, R.K., 2016. Numerical simulation of long-term storage of CO_2 in Yanchang shale reservoir of the Ordos basin in China. Chem. Geol. 440, 288–305.
Liu, D., Li, Y., Yang, S., Agarwal, R.K., 2019. CO_2 sequestration with enhanced shale gas recovery. Energy Sources, Part A Recovery, Util. Environ. Eff. 1–11.
Liu, F., Lu, P., Griffith, C., Hedges, S.W., Soong, Y., Hellevang, H., Zhu, C., 2012. CO_2–brine–caprock interaction: reactivity experiments on Eau Claire shale and a review of relevant literature. Int. J. Greenhouse Gas Control 7, 153–167.
Luo, X., Ren, X., Wang, S., 2019. Supercritical CO_2-water-shale interactions and their effects on element mobilization and shale pore structure during stimulation. Int. J. Coal Geol. 202, 109–127.
Manz, K.E., Carter, K.E., 2018. Degradation of hydraulic fracturing additive 2-butoxyethanol using heat activated persulfate in the presence of shale rock. Chemosphere 206, 398–404.
Marcon, V., Joseph, C., Carter, K.E., Hedges, S.W., Lopano, C.L., Guthrie, G.D., Hakala, J. A., 2017. Experimental insights into geochemical changes in hydraulically fractured Marcellus Shale. Appl. Geochem. 76, 36–50.
Marcon, V., Kaszuba, J.P., 2015. Carbon dioxide–brine–rock interactions in a carbonate reservoir capped by shale: experimental insights regarding the evolution of trace metals. Geochem. Cosmochim. Acta 168, 22–42.
Middleton, R.S., Carey, J.W., Currier, R.P., Hyman, J.D., Kang, Q., Karra, S., Jiménez-Martínez, J., Porter, M.L., Viswanathan, H.S., 2015. Shale gas and non-aqueous fracturing fluids: opportunities and challenges for supercritical CO_2. Appl. Energy 147, 500–509.
Mikutta, R., Kleber, M., Kaiser, K., Jahn, R., 2005. Review: organic matter removal from soils using hydrogen peroxide, sodium hypochlorite, and disodium peroxodisulfate. Soil Sci. Soc. Am. J. 69, 120–135.
Moniz, E.J., Jacoby, H.D., Meggs, A., Armstrong, R., Cohn, D., Connors, S., Deutch, J., Ejaz, Q., Hezir, J., Kaufman, G., 2011. The Future of Natural Gas. Massachusetts Institute of Technology, Cambridge, USA.
Morel, F., Hering, J., 1993. Principles and Applications of Aquatic Chemistry. John Wiley, New York, NY, USA.
Moses, C.O., Herman, J.S., 1991. Pyrite oxidation at circumneutral pH. Geochem. Cosmochim. Acta 55, 471–482.
Moses, C.O., Nordstrom, D.K., Herman, J.S., Mills, A.L., 1987. Aqueous pyrite oxidation by dissolved oxygen and by ferric iron. Geochem. Cosmochim. Acta 51, 1561–1571.
Pan, Y., Hui, D., Luo, P., Zhang, Y., Zhang, L., Sun, L., 2018. Influences of subcritical and supercritical CO_2 treatment on the pore structure characteristics of marine and terrestrial shales. J. CO2 Util. 28, 152–167.
Parmesan, C., 2006. Ecological and evolutionary responses to recent climate change. Annu. Rev. Ecol. Evol. Syst. 37, 637–669.
Paukert Vankeuren, A.N., Hakala, J.A., Jarvis, K., Moore, J.E., 2017. Mineral reactions in shale gas reservoirs: barite scale formation from reusing produced water as hydraulic fracturing fluid. Environ. Sci. Technol. 51, 9391–9402.
Pearce, J.K., Kirste, D.M., Dawson, G.K.W., Farquhar, S.M., Biddle, D., Golding, S.D., Rudolph, V., 2015. SO_2 impurity impacts on experimental and simulated CO_2–water–reservoir rock reactions at carbon storage conditions. Chem. Geol. 399, 65–86.
Pei, P., Ling, K., He, J., Liu, Z., 2015. Shale gas reservoir treatment by a CO_2-based technology. J. Nat. Gas Sci. Eng. 26, 1595–1606.
Phan, T.T., Paukert Vankeuren, A.N., Hakala, J.A., 2018. Role of water−rock interaction in the geochemical evolution of Marcellus Shale produced waters. Int. J. Coal Geol. 191, 95–111.
Pokrovsky, O.S., 2001. Kinetics and mechanisms of dolomite dissolution in neutral to alkaline solutions revisited. Am. J. Sci. 301, 597–626.
Rahm, D., 2011. Regulating hydraulic fracturing in shale gas plays: the case of Texas. Energy Policy 39, 2974–2981.

Salmon, V., Derenne, S., Lallier-Vergès, E., Largeau, C., Beaudoin, B.J.O.G., 2000. Protection of organic matter by mineral matrix in a Cenomanian black shale. Org. Geochem. 31, 463–474.
Saouma, V.E., Martin, R.A., Hariri-Ardebili, M.A., Katayama, T., 2015. A mathematical model for the kinetics of the alkali–silica chemical reaction. Cement Concr. Res. 68, 184–195.
Soler, J.M., 2003. Reactive transport modeling of the interaction between a high-pH plume and a fractured marl: the case of Wellenberg. Appl. Geochem. 18, 1555–1571.
Tamura, H., Goto, K., Yotsuyanagi, T., Nagayama, M., 1974. Spectrophotometric determination of iron(II) with 1,10-phenanthroline in the presence of large amounts of iron(III). Talanta 21, 314–318.
Thomas, M., 2011. The effect of supplementary cementing materials on alkali-silica reaction: a review. Cement Concr. Res. 41, 1224–1231.
Wang, L., Burns, S., Giammar, D.E., Fortner, J.D., 2016. Element mobilization from Bakken shales as a function of water chemistry. Chemosphere 149, 286–293.
Wang, L., Fortner, J.D., Giammar, D.E., 2015. Impact of water chemistry on element mobilization from eagle ford shale. Environ. Eng. Sci. 32, 310–320.
Wilke, F.D.H., Vieth-Hillebrand, A., Naumann, R., Erzinger, J., Horsfield, B., 2015. Induced mobility of inorganic and organic solutes from black shales using water extraction: implications for shale gas exploitation. Appl. Geochem. 63, 158–168.
Williams, B.H., 1928. The thermal decomposition of hydrogen peroxide in aqueous solutions. Trans. Faraday Soc. 24, 245–255.
Yang, Q., Matter, J., Takahashi, T., Stute, M., O'Mullan, G., Clauson, K., Umemoto, K., Goldberg, D., 2015. Groundwater geochemistry in bench experiments simulating CO_2 leakage from geological storage in the Newark Basin. Int. J. Greenhouse Gas Control 42, 98–108.
Yu, Z., Liu, L., Yang, S., Li, S., Yang, Y., 2012. An experimental study of CO_2–brine–rock interaction at in situ pressure–temperature reservoir conditions. Chem. Geol. 326–327, 88–101.
Zhang, H., Xiong, Z., Ji, F., Lai, B., Yang, P., 2017. Pretreatment of shale gas drilling flowback fluid (SGDF) by the microscale Fe^0/persulfate/O_3 process (mFe^0/PS/O_3). Chemosphere 176, 192–201.
Zhao, J., Jin, Z., Jin, Z., Wen, X., Geng, Y., 2017. Origin of authigenic quartz in organic-rich shales of the wufeng and Longmaxi formations in the Sichuan Basin, south China: implications for pore evolution. J. Nat. Gas Sci. Eng. 38, 21–38.
Zhou, Y., Lei, Y., Chen, W., Yu, W., 2018. Enhance low temperature oxidization of shale gas recovery using hydrogen peroxide. J. Pet. Sci. Eng. 164, 523–530.
Zhu, X., Cai, J., Liu, W., Lu, X., 2016. Occurrence of stable and mobile organic matter in the clay-sized fraction of shale: significance for petroleum geology and carbon cycle. Int. J. Coal Geol. 160–161, 1–10.
Zou, Y., Li, S., Ma, X., Zhang, S., Li, N., Chen, M., 2018. Effects of CO_2–brine–rock interaction on porosity/permeability and mechanical properties during supercritical-CO_2 fracturing in shale reservoirs. J. Nat. Gas Sci. Eng. 49, 157–168.